Journal of Power Sources 185 (2008) 559–565

Contents lists available at ScienceDirect

Journal of Power Sources

journal homepage: www.elsevier.com/locate/jpowsour

# A new lead alloy current-collector manufactured by a powder rolling process and its corrosion behavior under lead-acid battery conditions

Masanori Sakai [a,*], Yasuo Kondo [b], Satoshi Minoura [a], Takeo Sakamoto [a], Tokiyoshi Hirasawa [a]

[a] *Advanced Battery Development Center, Shin-Kobe Electric Machinery Co., Ltd., 2200 Oka, Fukaya, Japan*
[b] *Hitachi Research Laboratory, Hitachi, Ltd., Japan*

ARTICLE INFO

*Article history:*
Received 1 April 2008
Received in revised form 29 May 2008
Accepted 4 June 2008
Available online 21 June 2008

*Keywords:*
Corrosion
Lead alloy
Powder rolling
Current collector
Lead-acid battery
Corrosion growth

ABSTRACT

A new powder rolling process for manufacturing current-collector sheets for lead-acid batteries has been developed. Gas-atomized lead–tin and lead–tin–calcium alloy powders obtained by a rapid solidification process in air were employed as raw materials for the powder rolling process. The corrosion behavior of powder-rolled lead–tin alloys with various compositions of tin has been investigated. A dipping corrosion test of square plain sheets of the alloys was performed in $H_2SO_4$ at 75 °C. The test was repeated up to 20 cycles with each cycle consisting of a controlled 10 mA $cm^{-2}$ oxidation current for 6 h and a rest under open circuit voltage for 6 h. The extent of corrosion–elongation and the appearance of the corroded surface of the tested specimens were the main observations. The corrosion–elongation of the corroded sheet of a powder-rolled lead alloy containing 1.5 wt% tin with ca. 200 μm initial thickness was less than 5%, whereas that of the corroded sheet of the cast-rolled lead alloy containing 1.5 wt% tin with the same initial thickness was 25–30% under the same corrosion test conditions. The corroded powder-rolled sheet of the 1.5 wt% tin lead alloy has uniform corrosion, but the cast-rolled sheet of lead alloy containing 1.5 wt% tin was much distorted and was perforated by the corrosion. Intergranular corrosion of the powder-rolled lead–tin alloys was much suppressed as compared with that of the cast-rolled lead–tin alloys.


## 1. Introduction

It is of great importance to enhance the durability of current collectors of lead-acid batteries for emerging automotive applications, such as power-assisted hybrid automobiles, that require energy storage devices capable of delivering high specific power and high specific energy [1–3]. The development of thinner and lighter current collectors is aimed at providing batteries with both high specific power and high specific energy [4–6]. In order to ensure that current collectors are able to retain their functionality during their service life despite the effects of corrosion, the thickness of positive plate current collectors of lead-acid batteries has been, for example, ca. 1000 μm, for automobiles and more than a few millimeters for trickle charge applications. Provided that a high durability current collector, with high corrosion resistance, which is independent of thickness, is developed, the range of utility of lead-acid batteries can be improved. Alloy and grid technology for lead-acid batteries has been developed for this purpose in several ways. Thin current-collector technologies [4–6], the effects of tin, barium, or calcium–tin on corrosion resistance [7–11], negative electrode corrosion [12], kinetics of precipitation hardening [13], microstructure or aging of calcium–tin lead alloys [14,15], and a copper mesh grid of a negative electrode [16] have all been reported. Corrosion growth has been also reported [17–19]. Simulations of grid design optimizations have been performed as well [20–22]. As for corrosion, many books have been published on the subject [23].

As described above, however, powder-rolled lead alloys for current collectors of lead-acid batteries have not hitherto been investigated. In this study, a powder rolling process has been newly applied to the manufacture of current collectors of lead-acid batteries, and the corrosion characteristics of powder-rolled sheets of lead alloys have been investigated by comparison with conventional alloys containing various weight percent, wt%, of tin in cast-rolled lead–tin alloys, and 0.08 wt% calcium–1.6 wt% tin in cast-rolled lead–calcium–tin alloy.

The powder-rolled alloys obtained in this study have demonstrated superior characteristics with regard to both the corrosion–elongation by corrosion growth and intergranular

* Corresponding author. Tel.: +81 48 546 1113; fax: +81 48 546 1137.
*E-mail address:* m.sakai@shinkobe-denki.co.jp (M. Sakai).

0378-7753/$ – see front matter © 2008 Elsevier B.V. All rights reserved.
doi:10.1016/j.jpowsour.2008.06.035

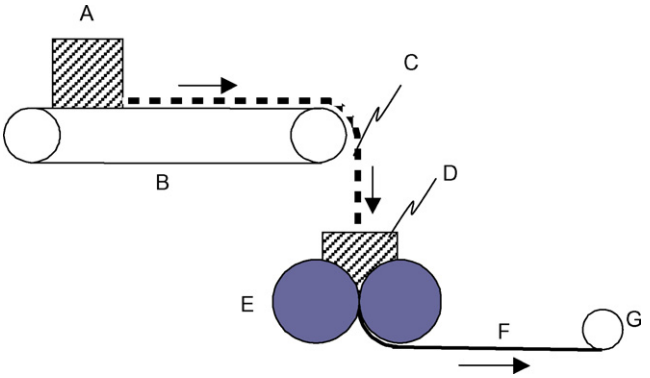


**Fig. 1.** A schematic diagram of a powder roll machine for current collectors of lead-acid batteries. A: 1st hopper; B: belt conveyor; C: atomized powder; D: 2nd hopper; E: compression roller; F: sheet of powder rolled; G: wind roller.

corrosion in comparison with those of the conventional alloys. Even with less than 100 μm thickness of metal phases remaining after the corrosion, tests of powder-rolled sheets have indicated no perforation under the test conditions.

## 2. Experimental

### 2.1. Powder rolling

Fig. 1 shows a schematic drawing of a powder rolling machine and Fig. 2 shows a photograph of a test-rolling machine. In Fig. 1, A is the 1st hopper, containing an atomized powder of lead alloys, B is the belt conveyor to move the atomized powder to the 2nd hopper, C is the atomized powder, D is the 2nd hopper, E is the compression roller of the atomized powder, F is the sheet of rolled powder, and G is the winding roller. In Fig. 2, A is the 1st hopper, B the compression rollers, and C the winding roller of the sheet of a powder-rolled alloy. A test-rolling machine developed by Ono Roll Co. was employed for powder rolling in this study. The powder rolling process for manufacturing lead-acid current collectors was performed according to the following processes: (1) An atomized-powder of a lead alloy was put in the first hopper with a slit of a few millimeters clearance installed on the belt conveyor

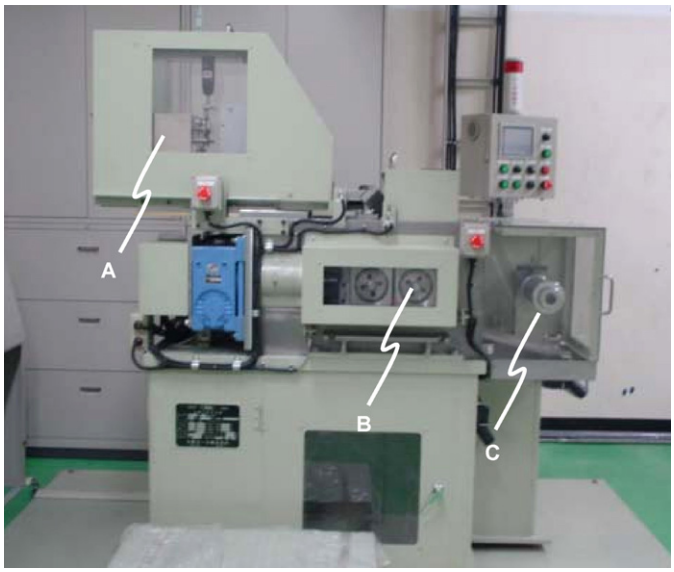


**Fig. 2.** A test powder roll machine for current collectors of lead-acid batteries. A: 1st hopper; B: compression roller; C: wind roller.

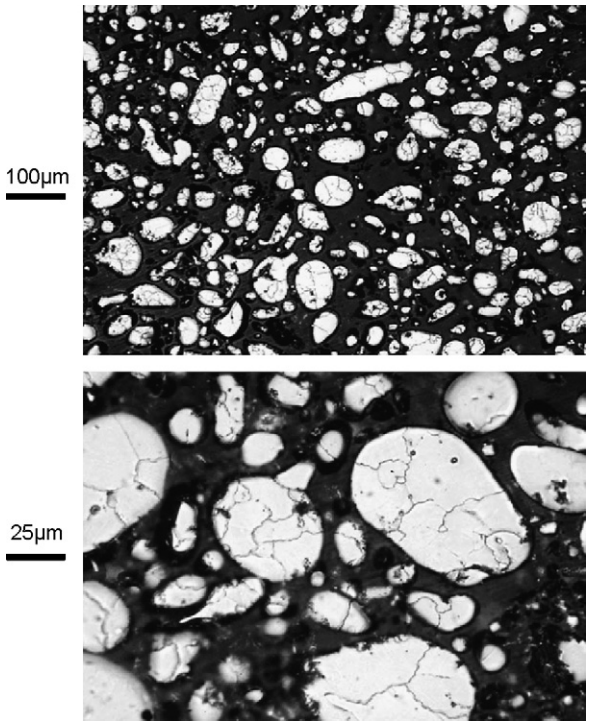


**Fig. 3.** Pb–1.5 wt%Sn atomized powder of raw materials for powder rolling.

in the figure. (2) After the rolling machine is turned on, the belt conveyor with atomized-powder starts to operate and two compression metal rollers facing each other horizontally start to rotate. (3) An atomized-powder on the belt conveyor is then dropped into the 2nd hopper, which is installed close to the two compression rollers as shown in Figs. 1 and 2. (4) A powder-rolled sheet issues from the clearance between the two compression rollers. The thickness of the powder-rolled sheet is usually less than 1 mm. Then the sheet of powder-rolled alloy is rolled up by the winding roller as shown in Figs. 1 and 2. The powder rolling of the atomized-powder of lead alloys was done under ambient temperature conditions. In this study, the powder rolling was performed twice. The first rolled sheet was 0.5 mm thick, and the second rolling reduced the thickness to 0.2 mm. In order to compare the corrosion behavior of the powder-rolled alloys with that of conventional alloys, Pb–1.5%Sn and Pb–0.08%Ca–1.6%Sn cast-rolled alloys were employed as reference alloys and were compressed by the second rolling process from 0.8 mm initial thick to 0.2 mm.

### 2.2. Raw materials for powder-rolled alloys

High-pressure air-cooled atomized powders of lead–tin alloys, containing 0.5, 0.75, 1.0, 1.25, 1.5, 1.75, and 2.5 wt%Sn were used. Fig. 3 shows a micrograph of the raw material powder of the 1.5 wt%Sn lead alloy. The sizes of the atomized-powders were limited to under 200 mesh. An atomized powder of a lead–calcium–tin alloy, (0.08 wt%Ca–1.6 wt%Sn), was also prepared under the same method as that for the Pb–Sn alloys. The surface oxidation of atomized powders was evaluated in terms of the total amount of oxygen contained in the powders by use of the inert gas fusion method.

### 2.3. Corrosion test and corrosion test specimens

Fig. 4 shows an example of one of the powder-rolled sheets rolled up, with the aid of the test-rolling machine, with dimensions 0.85 mm thickness, 150 mm width, and 9000 mm length. Fig. 5


**Fig. 4.** 1.5 wt%Sn lead alloy sheet wound up by the test powder roll machine.

shows a schematic of the corrosion test specimen used in this study. The corrosion test specimens were 10 mm wide, 40 mm long, and 0.2 mm thick. Fig. 6 shows the cross-section of the cylindrical test cell used in the corrosion test. Each specimen was dipped in 400 $cm^3$ of 1.28 specific gravity $H_2SO_4$ in a cylindrical beaker cell at 75 °C. The part of the working electrode (i.e. the part that was not immersed in the solution) was covered with an electrical insulated tape of the PTFE (NITOFLON® developed by Nitto Denko Co., Japan). Counter negative electrodes of the corrosion test specimens were employed, which were larger in area than the test specimens and were previously formed. Fig. 7 shows the program of the corrosion cycle test. One cycle of the corrosion test consists of 6-h charge and

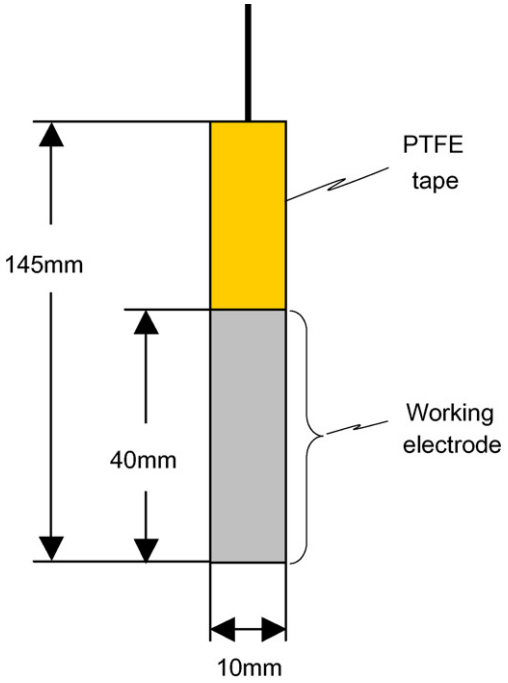


**Fig. 5.** 0.2 mm thick specimen plane diagram for the corrosion cycle test.

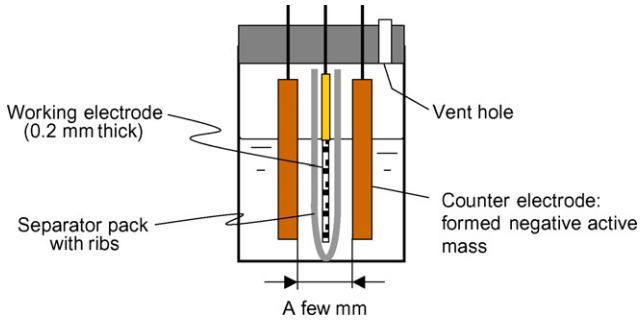


**Fig. 6.** Cross-section of cylindrical test cell for the corrosion cycle tests.

6-h rest under open circuit conditions. A controlled charging current of 10 mA $cm^{-2}$ was employed. Tests of either 14 or 20 cycles were mainly employed for continuous corrosion cycle tests. In order to observe metallographically the surface morphology, 1.5 wt%Sn powder-rolled and cast-rolled sheet were etched by using acetic acid/hydrogen peroxide of volume ratio 3/1.

### 2.4. Evaluation of corrosion test

A slide caliper was used to measure the length of corrosion test specimens before and after the tests in order to evaluate corrosion–elongation of specimens. The overall length of a specimen after distortion by the corrosion tests was defined as the projected length of the specimen in the direction of a rolling, which is the relative increase of the linear dimension. Care was taken not to stretch specimens after corrosion distortion. The thickness of a specimen after corrosion tests was measured by use of laser microscopy (developed by Lasertec Co.) whose precision was more than 1 μm. In order to evaluate the corrosion depth of specimens and to measure the thickness of the remaining metal phase in the specimens after corrosion cycle tests, specimens were embedded in an epoxy resin mold and metallographic cross-sections were polished to a 1-μm $Al_2O_3$ paste finish. The corrosion depth, the elongation rate of the corrosion–elongation by corrosion growth, and the corrosion rate were defined as follows:

$$\text{Corrosion depth } (\mu\text{m}) : \text{IT} - \text{RT} \quad (1)$$

$$\text{Elongation rate } (\%) : \frac{100(\text{IL} - \text{LA})}{\text{IL}} \quad (2)$$

$$\text{Corrosion rate } (\%) : \frac{100(\text{IT} - \text{RT})}{\text{IT}} \quad (3)$$

where IT is the initial thickness, RT the remaining metal phase thickness after the corrosion tests, IL the initial length, and LA the length after the corrosion tests.

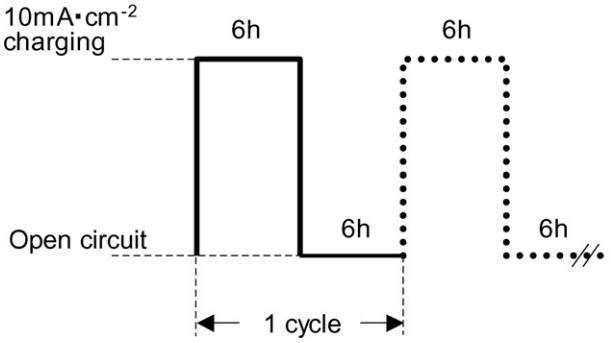


**Fig. 7.** Programs of corrosion cycle test.

**Table 1**
Corrosion depths and elongation rates of various specimens for the corrosion cycle tests

| Type of rolling | Lead alloy (wt%) | Cycle 14 | | | | Cycle 20 | | | |
|---|---|---|---|---|---|---|---|---|---|
| | | Corrosion depth (μm) | | Elongation rate (%) | | Corrosion depth (μm) | | Elongation rate (%) | |
| Powder-rolled | 0.5Sn | 119 | 116 | 1.9 | 2.1 | 178 | 176 | 5.7 | 5.9 |
| | 0.75Sn | 109 | 111 | 1.8 | 2.0 | 159 | 155 | 4.6 | 4.0 |
| | 1.0Sn | 107 | 108 | 2.2 | 1.9 | 149 | 148 | 4.3 | 3.5 |
| | 1.25Sn | 102 | 101 | 2.4 | 1.8 | 147 | 151 | 4.1 | 3.7 |
| | 1.5Sn | 98 | 98 | 1.9 | 1.5 | 151 | 149 | 3.8 | 4.3 |
| | 1.75Sn | 99 | 97 | 1.7 | 2.1 | 142 | 137 | 2.7 | 3.4 |
| | 2.5Sn | 93 | 97 | 2.0 | 2.0 | 133 | 130 | 3.0 | 3.5 |
| | 0.08Ca–1.6Sn | 115 | 117 | 2.0 | 2.0 | 160 | 160 | 3.3 | 2.3 |
| Cast-rolled | 1.5Sn | 134 | 138 | 17.2 | 15.6 | 198 | 199 | 31.9 | 38.1 |
| | 0.08Ca–1.6Sn | 113 | 110 | 2.2 | 3.0 | 200 | 200 | 3.3 | 3.7 |

Laser microscopy measurements were made 10 times at four arbitrarily selected locations on each corroded specimen. The mean corrosion depth of each specimen was taken as the average of the forty data measured by the laser microscope. A laser micrograph was used for the evaluation of surface unevenness after the corrosion tests as well.

## 3. Results and discussion

Table 1 shows the results of the corrosion tests for the 14 and the 20 cycle tests. The mean corrosion depth and the mean elongation rate due to corrosion growth are tabulated for each alloy composition, and the two data for each alloy correspond to the 14 cycle and 20 cycle tests, respectively. Fig. 8 shows cross-sectional views of corroded specimens for the corrosion cycle 14 test. The initial lengths of the specimens were 194–206 μm. The surface morphology of each specimen in Fig. 8 is seemingly the same except for the cast-rolled 1.5% Sn alloy, which was distorted much more than the others. Small scratches appearing on their surfaces are ascribed to the polishing of the surfaces of specimens. Fig. 9 shows the photographs of specimens after completion of the corrosion test of the cycle 14. Except for the cast-rolled lead alloy containing 1.5 wt%Sn, each specimen seems to retain its initial length. The corrosion growth of the cast-rolled specimen containing 1.5 wt%Sn was clearly visible to the naked eye.

Fig. 10 shows the relationship between the mean corrosion depth and the tin compositions of Pb–Sn alloys after completion of the corrosion test of the cycle 14. On the basis of the findings in Fig. 10, the mean corrosion depth is at a minimum at around 2 wt% of Sn. As shown in Fig. 10, the cast-rolled alloy containing 1.5 wt%Sn indicated ca. 1.5 times higher corrosion depth than that of the powder-rolled alloy containing 1.5 wt%Sn. Fig. 11 shows the relationship between the elongation rate and the tin compositions of both powder-rolled and the conventional cast-rolled specimens after completion of the corrosion test of the cycle 14 tests. Each pair of bars appearing in the figure corresponds to two specimens, which

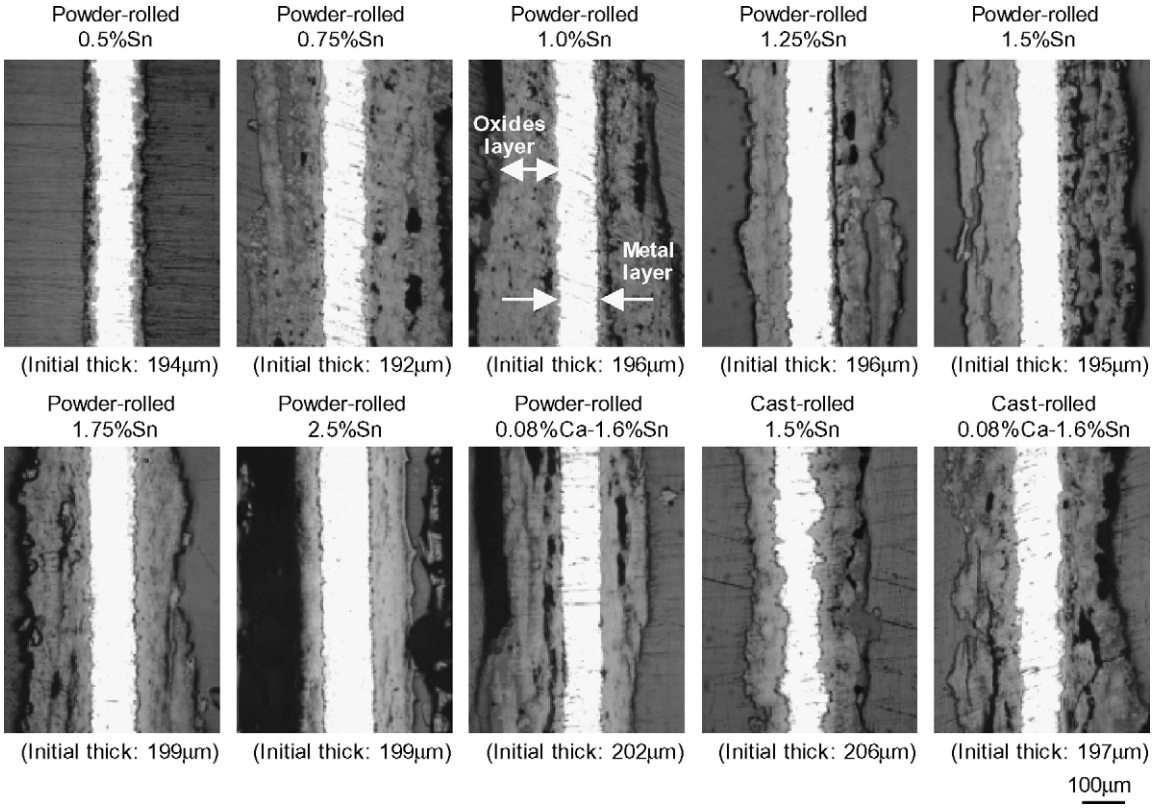


**Fig. 8.** Cross-sectional views of various corroded alloys after the corrosion test cycle 14.

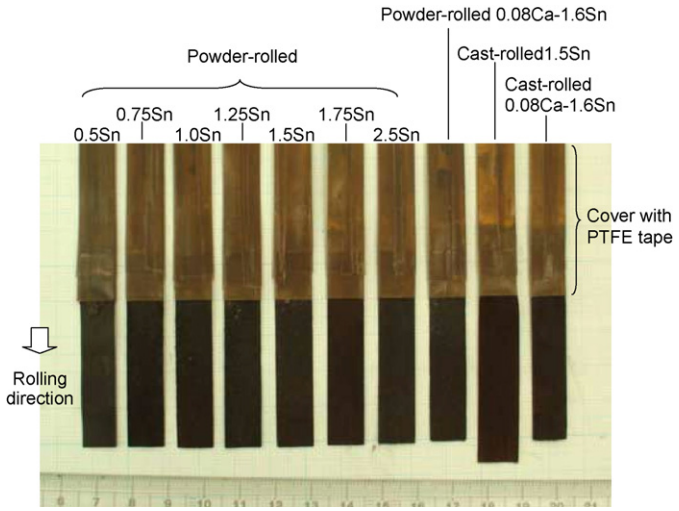


**Fig. 9.** Overviews of corroded specimens after the corrosion test cycle 14.

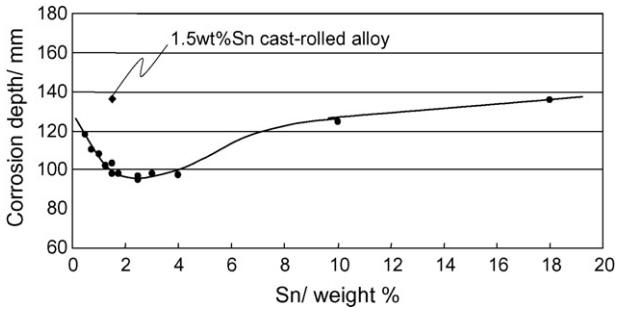


**Fig. 10.** Corrosion depth versus various Sn compositions of powder-rolled alloys after the corrosion test cycle 14.

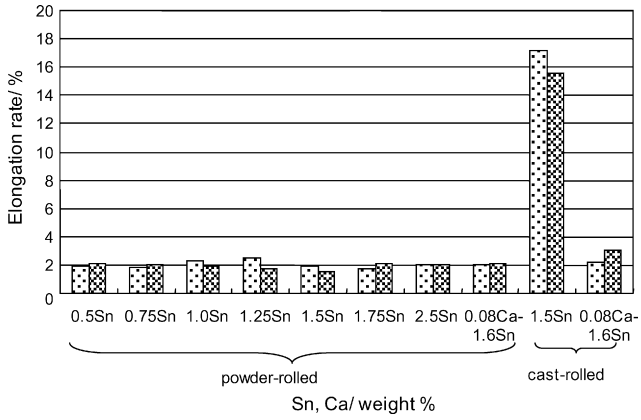


**Fig. 11.** Elongation rate versus various powder-rolled and cast-rolled alloys after the corrosion test cycle 14.

are of the same tin composition. As shown in Fig. 11, the elongation rate of the cast-rolled alloy containing 1.5 wt%Sn was nearly one order of magnitude higher than those of the powder-rolled alloys. Except for the cast lead alloy containing 1.5 wt%Sn, the elongation rates for the powder-rolled alloys were all around 2% at cycle 14 of the corrosion test.

Fig. 12 shows cross-sectional views of corroded specimens after cycle 20 of the corrosion test. The surface morphology of each specimen was seemingly the same except for three specimens: the cast-rolled alloys of both 1.5% Sn and 0.08 wt%Ca–1.6 wt%Sn and the 0.5 wt%Sn powder-rolled alloy. The two specimens of the cast-rolled alloys containing 1.5%Sn and 0.08 wt%Ca–1.6 wt%Sn were perforated by the corrosion. The powder-rolled alloy containing 0.5 wt%Sn demonstrated unevenness of the remaining metal surface although it did not show any perforation by corrosion like that

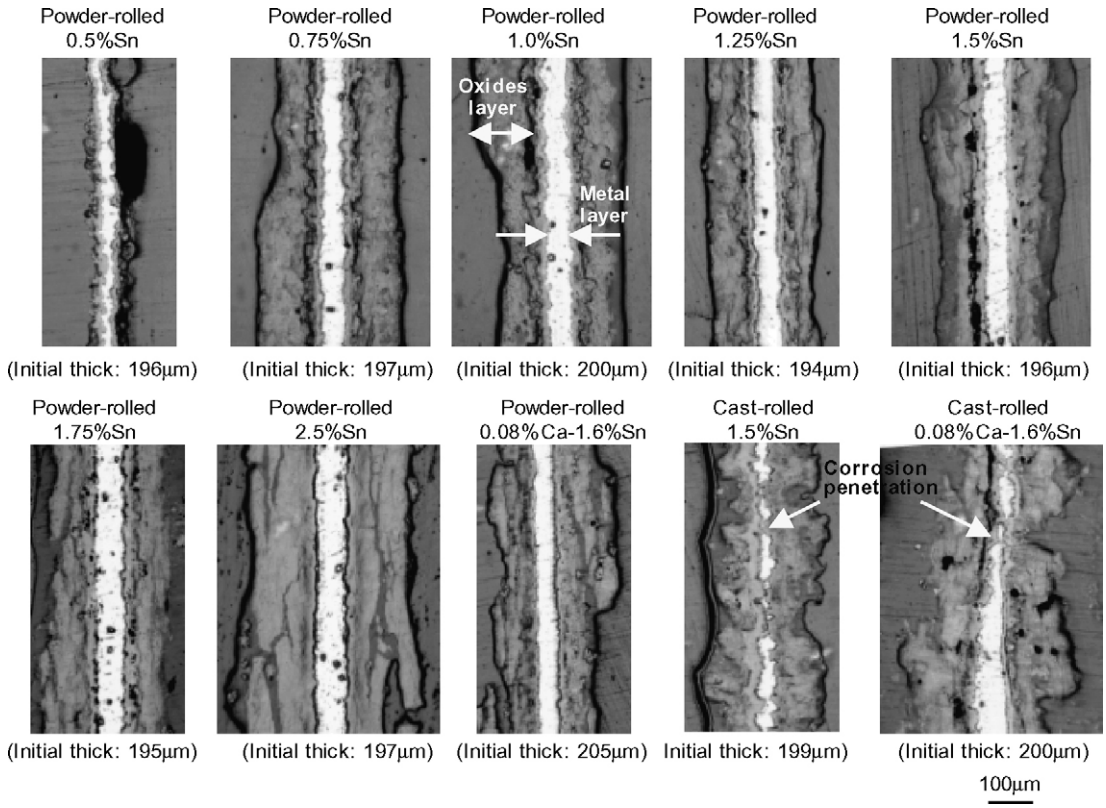


**Fig. 12.** Cross-sectional views of various corroded alloys after the corrosion test cycle 20.

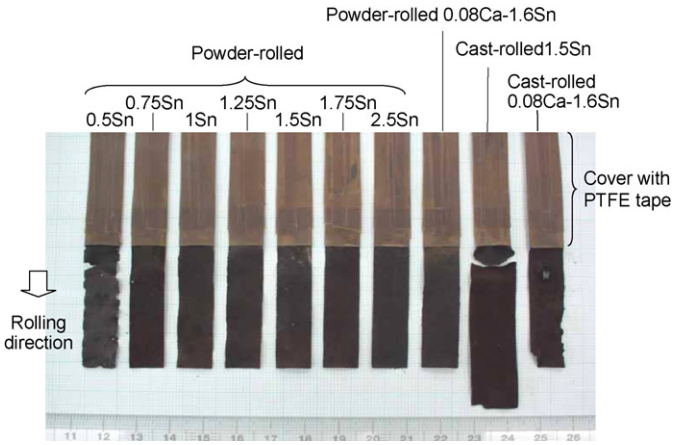


**Fig. 13.** Overviews of corroded specimens after the corrosion test cycle 20.

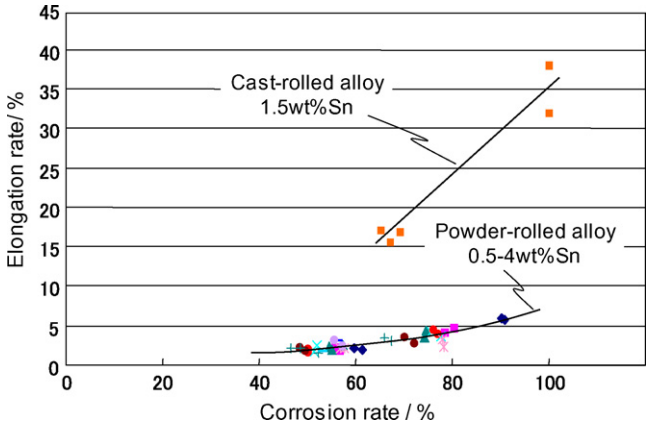


**Fig. 15.** Elongation rate versus corrosion rate under various corrosion rates conditions.

seen in the cast-rolled alloys. The initial thicknesses of each specimen for the corrosion of both cycles 14 and 20 were 194–205 μm. The initial thicknesses of the specimens having the same alloy compositions for the corrosion test of cycles 14 and 20 were the same as each other because each specimen having the same alloy composition for the corrosion test of cycle 14 and 20 were made from the same prepared sheet of alloys.

Fig. 13 shows photographs of specimens after the corrosion test of cycle 20. Elongation due to corrosion growth appears on the conventional cast-rolled alloy containing 1.5 wt%Sn and, as shown in the figure, an intergranular corrosion divided the specimen into two pieces. For the 0.08 wt%Ca-1.6 wt%Sn cast-rolled alloy, the corrosion-elongation measured by the projected length was small. As shown in Fig. 12, however, several locations of the specimen revealed corrosion perforation and its surface was much distorted. In Fig. 13, the 0.5 wt%Sn powder-rolled alloy also exhibited surface unevenness and one portion of the specimen was displaced during the manipulation of the specimen after the corrosion test.

Fig. 14 shows the relationship between the elongation rate and the tin content of powder-rolled alloys and the 1.5 wt% cast-rolled alloy. The elongation rates of the powder-rolled specimens were all small as compared with those of the 1.5 wt%Sn cast-rolled alloy. Fig. 15 shows the relationship between the elongation rate and the corrosion rate including data for corrosion cycles 14 and the 20. Fig. 16 shows the etched surfaces of the 1.5 wt%Sn powder-rolled and the 1.5 wt%Sn cast-rolled alloys. The perpendicular directions to the etched surfaces in Fig. 16 are those of powder rolling.

As was demonstrated above, the corrosion behavior of powder-rolled alloys was inherently different from that of the conventional

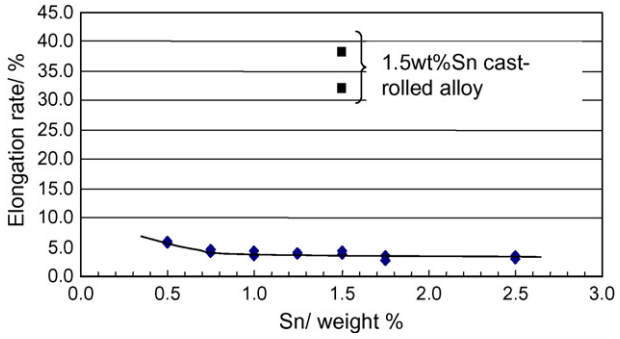


**Fig. 14.** Elongation rate versus various powder-rolled and cast-rolled 1.5 wt%Sn alloys after the corrosion test cycle 20.

cast-rolled alloys. As shown in Figs. 11 and 12, the cast-rolled alloy containing 1.5 wt%Sn demonstrated an elongation rate that was one order magnitude higher than that of the powder-rolled alloys. For the 0.08 wt%Ca–1.6 wt%Sn cast-rolled alloy, although the cross-sectional views of the alloy in Figs. 5 and 9 seemed to be comparable to those of the powder-rolled alloys up to cycle 14 of the corrosion test, the view of the 0.08 wt%Ca–1.6 wt%Sn cast-rolled alloy turned to be different from that of powder-rolled alloys at cycle 20. Thus, up to cycle 14, the 0.08 wt%Ca–1.6 wt%Sn cast-rolled alloy demonstrated robustness against intergranular corrosion and corrosion growth. At the corrosion test of cycle 20, however, the cast-rolled alloy showed corrosion perforation and, as Fig. 13 shows, the surface appearance was much distorted by corrosion growth. On the other hand, the powder-rolled alloys containing tin from 0.75 to 2.5 wt% still demonstrated their robustness against corrosion growth and intergranular corrosion, as shown in Figs. 9 and 10. Especially around 2 wt%Sn the compositions of the powder-rolled alloys, demonstrated superior robustness. That is, under the corrosion test conditions of cycle 20, even though less than 100 μm of metal phase remained as a current collector indicating more than 70% of material lost by corrosion, the powder-rolled alloy sheets still demonstrated high stability with no distinct distortion and no distinct corrosion growth. In general, the phenomenon of corrosion growth of lead alloys involved several factors [17–19,23]: alloy mechanical strength, oxide corrosion films on the metal surface, crystal grain size, and segregation of lead–tin compounds as impurity in intergranular or transgranular regions. Under the conditions of the corrosion tests performed herein, corrosion products of the lead alloys were essentially lead dioxide, $PbO_2$. Thus the phase change from Pb to $PbO_2$ needs volume increase, which is considered to be the essential force-giving rise to corrosion growth. The tensile strength of the cast-rolled and the powder-rolled Pb–Sn alloys containing 1.5 wt%Sn was 18.9 and 27.8 N mm$^{-2}$, respectively. Then, the tensile strength of the 0.08 wt%Ca–1.6 wt%Sn cast-rolled alloy is about two times higher than that of the 1.5 wt%Sn cast-rolled alloy. The robustness of the 0.08 wt%Ca–1.6 wt%Sn cast-rolled alloy against corrosion growth, thus, seems to be related to the strength of the material itself. However, the powder-rolled alloys have demonstrated superior robustness to that of the 0.08 wt%Ca–1.6 wt%Sn cast-rolled alloy. These findings have been considered as follows:

According to the so-called the Hall–Petch rule by Eq. (4), material strength is proportional to the reciprocal value of the square root of the size of crystal grains.

$$\sigma_y = \sigma_0 + \alpha G^{-1/2} \quad (4)$$

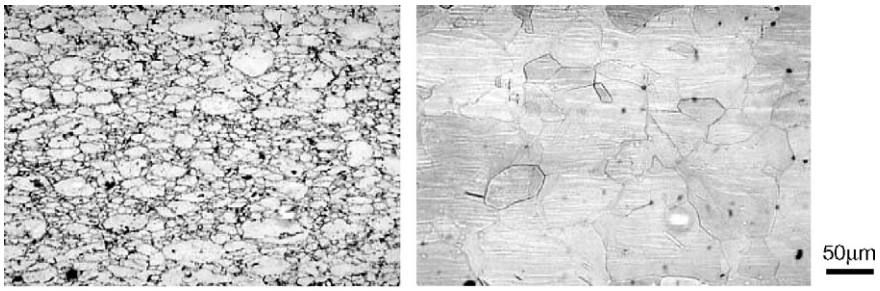


**Fig. 16.** Surface morphologies of metallographically etched alloys of powder-rolled and cast-rolled 1.5 wt%Sn.

where $\sigma_y$ is the yield stress, $\sigma_0$ the material constant, $\alpha$ the material constant, and $G$ the crystal grain size. By Eq. (4), if the compositions of materials are the same, the strength of a smaller grain size material is expected to be higher than that of a larger grain size material. As Fig. 16 shows, the grain sizes of the powder-rolled and the cast-rolled alloy containing 1.5 wt%Sn, revealed metallographically by etching, are quite different from each other and those of the powder-rolled alloy are smaller than those of the cast-rolled alloy. The sizes of the powder-rolled grains of the raw materials appearing in Fig. 3 and the grain distribution in Fig. 16 is seen to be similar, although rolled the powder grains are distorted in Fig. 16. On the basis of the surface morphologies of the metallographically etched alloys, as Fig. 16 shows, recrystallization of the grains of the powder-rolled alloys was much less than that of cast-rolled alloys. This apparent pinning effect of the powder-rolled alloys on the growth of crystal grains was considered to be an inherent characteristic of the powder-rolled lead-alloys. According to the analytical data by the inert gas fusion method, the mean value of the total amount of oxygen involved in atomized powders of the raw material for the powder-rolled Pb–Sn alloy containing 1.5 wt%Sn was 439 ppm. Therefore, it can be clearly understood that the raw materials of atomized powders contain lead oxides formed by the oxidation in air and these oxides formed on the surface of atomized powders play an important role for the pinning effect. It was considered that the uniformly distributed fine-scale segregations, inside the raw materials for the powder rolling, resulting from the rapid solidification process, and the naturally formed oxides on the surfaces of the raw powder materials under air and ambient temperature conditions, resulted in the robust corrosion resistance of the powder-rolled alloys.

The superior characteristic of suppressed corrosion–elongation behavior and high corrosion resistance appearing for the powder-rolled alloys shown herein seems to enable the manufacture of thin and light current collectors for lead-acid batteries.

## 4. Conclusions

(1) The corrosion–elongation of the powder-rolled Pb–Sn alloys was suppressed much more than that of the conventional cast-rolled lead alloys containing 1.5 wt%Sn and 0.08 wt%Ca–1.6 wt%Sn.
(2) The corrosion–elongation rate of the powder-rolled alloy sheet containing 1.5 wt%Sn, having the initial thick of ca. 200 μm, was one order of magnitude less than that of the cast-rolled lead alloy containing 1.5 wt%Sn.
(3) Powder-rolled sheet alloy around 2 wt%Sn compositions of Pb–Sn alloys have especially demonstrated superior robustness with no distinct distortion, no distinct corrosion growth, and no corrosion perforation under the corrosion test conditions.

## Acknowledgments

Thanks are expressed to Ms. K. Honbou and Dr. Y. Aono of Hitachi Research Laboratory, Hitachi Ltd. and Mr. H. Tada of Shin-Kobe Electric Machinery Co., Ltd. for helpful discussions.

## References

[1] P.T. Moseley, D.A.J. Rand, J. Power Sources 133 (2004) 104–109.
[2] P.T. Moseley, R.F. Nelson, A.F. Hollenkamp, J. Power Sources 157 (2006) 3–10.
[3] P.T. Moseley, Proceedings of the Seventh International Advanced Automotive Battery & Ultracapacitor Conference, Produced by Advanced Automotive Batteries, Long Beach, CA, USA, May 16–18, 2007.
[4] R.C. Bhardwaj, J. Power Sources 78 (1999) 130–138.
[5] R.C. Bhardwaj, T. John, J. Power Sources 91 (2000) 51–61.
[6] A. Caballero, M. Cruz, L. Hernan, J. Morales, L. Sanchez, J. Power Sources 125 (2004) 246–255.
[7] G. Bourguignon, A. Maitre, E. Rocca, J. Steinmetz, L. Torcheux, J. Power Sources 113 (2003) 301–307.
[8] J. Xu, X. Liu, X. Li, E. Barbero, C. Dong, J. Power Sources 155 (2006) 420–427.
[9] D. Slavkov, B.S. Haran, B.N. Popov, F. Fleming, J. Power Sources 112 (2002) 199–208.
[10] E. Rocca, G. Bourguignon, J. Steinmetz, J. Power Sources 161 (2006) 666–675.
[11] E. Jullian, L. Albert, J.L. Caillerie, J. Power Sources 116 (2003) 185–192.
[12] N. Koura, K. Kasuya, K. Ui, Y. Takiguchi, Y. Idemoto, Denki Kagaku 2 (2005) 135–140.
[13] M. Dehmas, A. Maitre, J.B. Richir, P. Archambault, J. Power Sources 159 (2006) 721–727.
[14] I. Mukaitani, H. Tsubakino, L. Liu, A. Yamamoto, S. Fukumoto, J. Power Sources 158 (2006) 897–901.
[15] J.P. Hilger, A. Boulahrouf, Mater. Charact. 24 (1990) 159–167.
[16] M. Lushina, Y. Kamenev, V. Leonov, E. Ostapenko, J. Power Sources 148 (2005) 95–104.
[17] H. Bode, in: R.J. Brodd, K.V. Kordesch (Eds.), Lead-Acid Batteries, John Wiley & Sons, Inc., 1977, pp. 345–346.
[18] I. Mukaitani, K. Hayashi, I. Shimoura, A. Takemasa, I. Takahashi, H. Tsubakino, J. Power Sources 144 (2005) 528–535.
[19] H. Warlimont, T. Hofmann, K. Jobst, J. Power Sources 144 (2005) 486–493.
[20] Y. Yang, W.M. Saslow, J. Chem. Phys. 109 (1998) 10331–10338.
[21] Y. Morimoto, Y. Ohya, K. Abe, T. Yoshida, H. Morimoto, J. Electrochem. Soc. 135 (1988) 293–298.
[22] K. Yamada, K. Maeda, K. Sasaki, T. Hirasawa, J. Power Sources 113 (2005) 352–357.
[23] D.A. Jones, Corrosion, Macmillan Publishing Company, New York, 1992, p. 19.